ARTICLE

UV Photodissociation Dynamics of Nitric Acid: The Hydroxyl Elimination Channel[†]

Feng-yan Wang, Zhi-chao Chen, Yong-wei Zhang, Quan Shuai, Bo Jiang, Dong-xu Dai, Xiu-yan Wang, Xue-ming Yang*

State Key Laboratory of Molecular Reaction Dynamics, Dalian Institute of Chemical Physics, Chinese Academy of Sciences, Dalian 116023, China

(Dated: Received on February 22, 2009; Accepted on March 17, 2009)

Sliced velocity mapping ion imaging technique was employed to investigate the dynamics of the hydroxyl elimination channel in the photodissociaiton of nitric acid in the ultraviolet region. The OH product was detected by (2+1) resonance enhanced multiphoton ionization via the $D^2\Sigma^-$ electronic state. The total kinetic energy spectra of the OH+NO_2 channel from the photolysis of $HONO_2$ show that both $NO_2(\widetilde{X}^2A_1)$ and $NO_2(\widetilde{A}^2B_2)$ channels are present, suggesting that both $1^1A''$ and $2^1A''$ excited electronic states of $HONO_2$ are involved in the excitation. The parallel angular distributions suggest that the dissociation of the nitric acid is a fast process in comparison with the rotational period of the HNO_3 molecule. The anisotropy parameter β for the hydroxyl elimination channel is found to be dependent on the OH product rotational state as well as the photolysis energy.

Key words: Slice imaging technique, Photodissociation dynamics, Nitric acid, OH radical, Resonance enhanced multiphoton ionization

I. INTRODUCTION

The hydroxyl radical is an important radical in the chemistry of the atmosphere. It is one of the most important oxidants in the troposphere acting as a "detergent" as it reacts with many pollutants [1]. Generally, there are two ways to detect the OH radical: laser-induced fluorescence (LIF) and resonance-enhanced multiphoton ionization (REMPI). The LIF method has been widely used in the study of the photodissociation dynamics of OH-containing molecules in the OH channel, while the REMPI technique has been rarely used.

A number of laser photoionization schemes have been used in the detection of the OH radical [2-9]. One commonly used scheme for OH detection is the (2+1) REMPI via the intermediate Rydberg $\widetilde{D}^2\Sigma^-$ and $3^2\Sigma^-$ states [2-6]. Alternatively, single vacuum ultraviolet (VUV) photons can also directly excite the OH radical to the $D^2\Sigma^-$ state followed by pulsed field ionization [7] or ultraviolet (UV) photon ionization [8,9]. In this work the (2+1) REMPI of OH via the $D^2\Sigma^-$ Rydberg state was used to study the photodissociation dynamics of nitric acid ($HONO_2$), in combination with slice ion imaging technique.

The OH production channel from photodissociation of nitric acid [10-20] in the UV region is of direct interest for astronomy or exobiology studies and has been extensively studied with the LIF method. As shown in Fig.1, The $HONO_2$ absorption spectrum shows a $n\rightarrow\pi^*(^1A'\rightarrow{}^1A'')$ transition peak at 36364 cm^{-1} (4.5 eV) and a $\pi\rightarrow\pi^*(^1A'\rightarrow{}^1A')$ transition peak near 54054 cm^{-1} (6.7 eV), localized on the NO_2 group [21-23]. At low excitation energy such as 35714 cm^{-1} (4.43 eV), it is suggested that the excitation of $HONO_2$ is vibronically coupled to the electronic transition $^1A'\rightarrow{}^1A''$ according to the Franck-Condon consideration from the ground planar geometry to the excited pyramidal geometry [17]. Although the photolysis of HNO_3 has been extensively studied in a wide range of photon energies, the mechanism of dissociation is still unclear with regard to the identification of the NO_2 product electronic states due to the mixing between the high vibrational levels of $\widetilde{X}^2A_1$ state with the $\widetilde{A}^2B_2$ state. Direct measurement of the electronic states of NO_2 is quite difficult as NO_2 would dissociate at the high internal energy above 25100 cm^{-1}.

This work will provide another look at the detailed dynamics of the nitric acid photodissociation by measuring the OH fragment with the sliced velocity mapping ion imaging technique at the three different photon energies indicated in Fig.1.

[†]Part of the special issue for "the 4th Sino-French Workshop on Molecular Spectroscopy, Dynamics and Quantum Control".

*Author to whom correspondence should be addressed. E-mail: xmyang@dicp.ac.cn

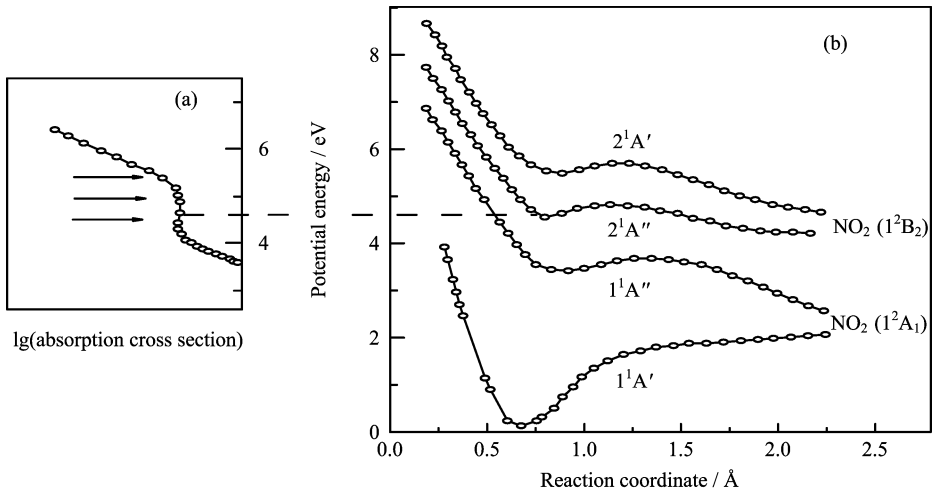

FIG. 1 Absorption cross section spectra of $HONO_2$ [21] (a) and Potential energy surfaces of HNO_3 along the reaction coordinate NO_2-OH [23] (b). Two peaks appear in the ultraviolet absorption spectra and three excited electronic states are involved in the region. The excited electronic states of $2^1A''$ and $2^1A'$ are correlated to $NO_2(1^2B_2)$+$OH(^2\Pi)$ [33] while the excited state of $1^1A''$ and the ground electronic state correlated to $NO_2(1^2A_1)$+$OH(^2\Pi)$ [23]. The arrows indicate the positions of the photolysis energies of $HONO_2$ used in this work.

II. EXPERIMENTS

The OH elimination channel from the photolysis of $HONO_2$ was studied in this work using the sliced velocity mapping ion imaging technique [24-27]. The experimental setup has been described previously in detail [28-30]. The design of the ion optics is similar to that reported by Lin *et al.* [26]. Briefly, the ion optics set is composed of 31 circular stainless plates, and is divided into a weak field region and a strong field region. The weak field region is used to extract ions and the strong field is used to accelerate ions. The molecular beam is formed by expanding an online mixed sample of HNO_3/He sample with a backing pressure of about 0.1 MPa into the vacuum chamber via a pulsed valve. The molecular beam is skimmed by a cone shaped skimmer and then intersected with two counter-propagating linearly polarized laser beams (the photolysis laser beam and the probe laser beam). The polarization of the photolysis laser is chosen to be parallel to the image plane, while the polarization of the probe laser can be rotated to be perpendicular to the image plane (VH geometry) or to be parallel to the image plane (VV geometry) using a quartz half-wave plate.

The $HONO_2$ molecule was dissociated by a tunable UV photolysis laser, and the OH fragment was detected via (2+1) REMPI at ∼244 nm by another UV probe laser. The OH ions were then projected onto a Chevron microchannel plate imaging detector (MCP). The position sensitive signals were then coupled out via a phosphor screen. Photon signals from the phosphor screen were recorded by a photomultiplier tube (PMT) and a CCD camera. By scanning the probe laser, the REMPI spectra of OH were measured. The OH product ion bunch produced by the UV laser pulse was expanded to about 200 ns in the ion optics before reaching the MCP detector. A time slicing window of about 40 ns was applied on the front MCP in order to obtain the sliced images. Doppler scan was made over whole OH rotational line profiles for taking the sliced images. The OH sliced images were symmetrized to extract the kinetic energy distribution and angular distribution. The translational energy was calibrated with the O^+ from the multiphoton dissociation/ionization of O_2 at 225 nm [31].

III. RESULTS AND DISCUSSION

A. OH REMPI spectra

Figure 2 shows the (2+1) REMPI spectra of OH via the $\widetilde{D}^2\Sigma^-$ Rydberg state, which were produced from the photolysis of $HONO_2$ in the one-color one-photon dissociation and three-photon ionization experiment. The ground state $^2\Pi$ of OH has two spin-orbit components, $^2\Pi_{3/2}$ and $^2\Pi_{1/2}$. The $^2\Pi_{3/2}$ component is the lowest member of the doublet, and the $^2\Pi_{1/2}$ component lies at 123 cm^{-1} above $^2\Pi_{3/2}$. The assignment to the REMPI spectra of OH ($X^2\Pi$) in the N'' ($N''=J''\pm1/2$, $N''>0$) level is shown at the top of Fig.2. Most of the OH rotational transitions are well resolved with only a few transitions overlapping with each other. Obviously, the appearance of $R_1(6)$ and $R_1(7)$ rotational transition from the photolysis of $HONO_2$ suggest that the OH fragment from the photolysis of $HONO_2$ is rotationally excited. Sliced images of the OH fragment in the different rotational states were recorded from the photolysis of $HONO_2$ at various excitation photon energies.

DOI:10.1088/1674-0068/22/02/191-196

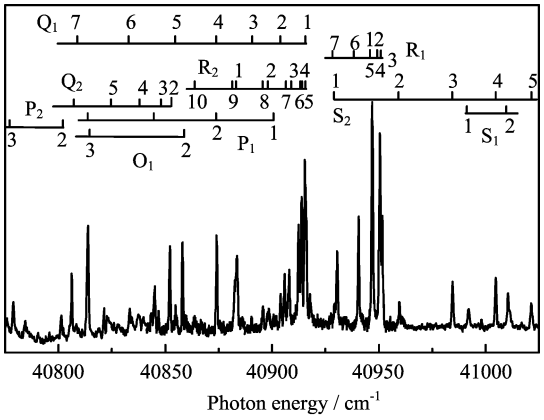

FIG. 2 The resolved rotational spectra of (2+1) REMPI of OH ($D^2\Sigma^-(N', v'=0) \leftarrow\leftarrow X^2\Pi(N'', v''=0)$) radical from the dissociation of $HONO_2$ in the one-color photodissociation and fragment ionization process. The assignment to the rotational transitions of OH ($X^2\Pi$, $N''=J''\pm1/2(N''>0)$) is shown at the top of the figure.

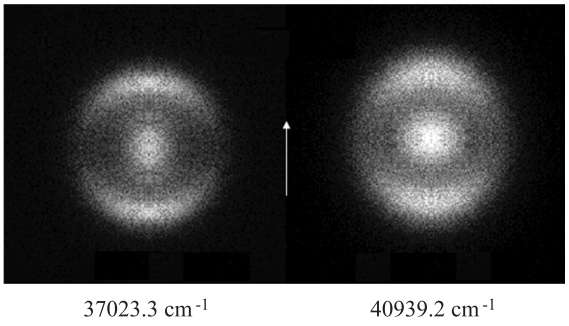

FIG. 3 The slice images of OH from photolysis of $HONO_2$ at 37023.3 and 40939.2 cm^{-1} with the (2+1) detection of OH at $R_1(6)$ transition. The arrows indicate both of the polarization direction of the photolysis laser and detection laser parallel to the detector.

B. Sliced images of OH product from photolysis of $HONO_2$

Sliced images of the OH fragment from the photolysis of $HONO_2$ at 37023 and 40939 cm^{-1} were recorded and are shown in Fig.3. The kinetic energy distributions of OH are obtained from the sliced images and converted into the total kinetic energy distribution of the OH+NO_2 products based on momentum conservation. The angular distribution is derived from the sliced images of OH by integrating the radial intensity in the range of 0°-180°. Anisotropy parameter β is obtained by fitting the angular distribution to the following equation:

$$I(\theta) \propto 1 + \beta P_2(\cos\theta) \quad (1)$$

where $P_2(\cos\theta)$ is the second Legendre polynomial, θ is the angle between the photofragment recoil velocity and the photolysis laser polarization direction, and β is in the limited region [2, −1]. In the limit of fast dissociation and axial recoil, β equals 2 or −1 when the transition dipole moment is parallel or perpendicular to the fragment recoil velocity respectively. Obviously, Figure 3 shows a parallel angular distribution of OH from photodissociation of $HONO_2$, suggesting that the anisotropy parameter is positive.

C. Kinetic energy distributions

The total kinetic energy distributions of the OH+NO_2 product were derived from the sliced images of the OH fragment and are shown in Fig.4. There is a very slow component in the TKER spectra and this is likely due to the cluster dissociation. The main feature in the spectra is clearly due to the hydroxyl elimination channel with its peak around 5000 cm^{-1} when the (2+1) REMPI is set at both $P_1(4)$ and $R_1(6)$ transitions. As the photolysis energy increases from 37023.3 cm^{-1} to 44924.8 cm^{-1}, an almost 1 eV increase, the peak position in the kinetic energy distribution does not seem to change much. This peak position is similar to the peak position of the slow component in the previous experimental study by Huber *et al.*, in which the mean translational energy for the slow component is 5500 cm^{-1} for the OH+NO_2 channel at 193 nm excitation [32]. The fast component is 13300 cm^{-1} for the same channel at 193 nm.

The dissociation energy for the OH+NO_2 pathway is 16500 cm^{-1}. NO_2 in the first excited electronic state lies at 9750 cm^{-1} above the ground state. As seen in Fig.4, the available energies for the $NO_2(\widetilde{X}^2A_1)$ and $NO_2(\widetilde{A}^2B_2)$ channels are indicated in the TKER spectra. All TKER spectra in Fig.4 show that the distributions extend to the limit of the $OH(X^2\Pi)$+$NO_2(\widetilde{X}^2A_1)$ channel. This means that the $OH(X^2\Pi)$+$NO_2(\widetilde{X}^2A_1)$ channel must be present. The distribution above the $OH(X^2\Pi)$+$NO_2(\widetilde{A}^2B_2)$ limit must come from the $OH(X^2\Pi)$+$NO_2(\widetilde{X}^2A_1)$ channel. The component peaked at about 5000 cm^{-1} probably comes mainly from the $NO_2(\widetilde{A}^2B_2)$ channel with some contribution from the $NO_2(\widetilde{X}^2A_1)$ channel. However, it is difficult to separate these two contributions in the experimentally obtained kinetic energy spectra. Therefore, the branching ratio between the two channels cannot be determined exactly from this experiment.

According to the *ab initio* calculations of the potential energy surfaces as shown in Fig.1, two electronic states, $1^1A''$ and $2^1A''$ states, are in the region of interest in our work [23]. The $1^1A''$ surface lies at about 27400 cm^{-1}, while the $2^1A''$ state lies at about 36600 cm^{-1}. The third excited electronic state from the $\pi\pi^*$ excitation (origin at 45732.7 cm^{-1}) is not energetically accessible in our experiment. From theory, the $1^1A''$ state is clearly correlated with

DOI:10.1088/1674-0068/22/02/191-196

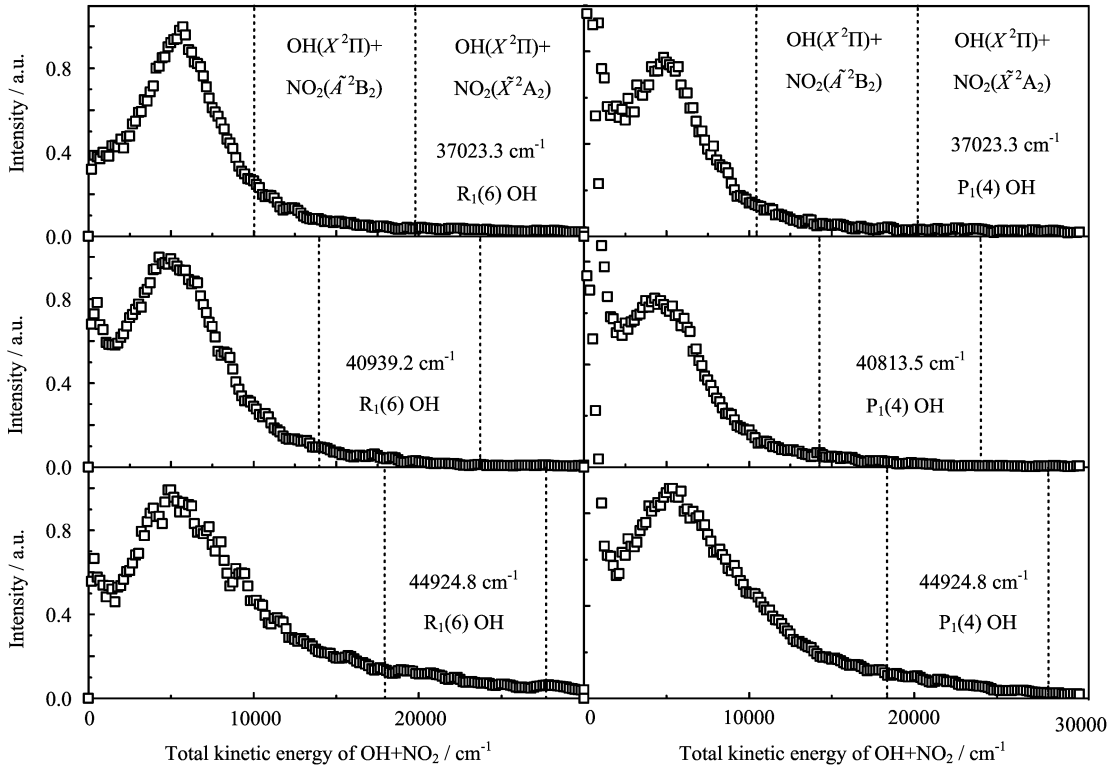

FIG. 4 Total kinetic energy distributions of OH($X^2\Pi$)+NO$_2$($\widetilde{X}^2$A$_1$, $\widetilde{A}^2$B$_2$) fragments produced from the photolysis of $HONO_2$ at the three photolysis energies with the (2+1) REMPI detection of OH at $R_1(6)$ and $P_1(4)$ transitions. The energy limit for the OH($X^2\Pi$)+NO$_2$($\widetilde{X}^2$A$_1$)/NO$_2$($\widetilde{A}^2$B$_2$) channels are shown by the dashed lines.

OH($X^2\Pi$)+NO$_2$($\widetilde{X}^2$A$_1$) and the $2^1A''$ state correlated with OH($X^2\Pi$)+NO$_2$($\widetilde{A}^2$B$_2$) [10,33]. Both of the excited state surfaces have a small barrier towards the dissociation due to the avoided crossing of $1^1A''$ and $2^1A''$ surfaces [23].

Obviously, the two excited $1^1A''$ and $2^1A''$ surfaces are in competition to lead to the respective NO$_2$($\widetilde{X}^2$A$_1$) and NO$_2$($\widetilde{A}^2$B$_2$) channels. The sudden increase in the absorption spectra beginning at ~41000 cm^{-1} suggests that the $2^2A''$ state is probably the major photoexcitation route above that energy. This implies that at the energy well below 41000 cm^{-1}, the $1^1A''$ state excitation is likely a major photoexcitation route. If this is the case, the OH($X^2\Pi$)+NO$_2$($\widetilde{X}^2$A$_1$) channel should be the major pathway at low photon energy excitation since the $1^1A''$ state correlates to this channel. Previous LIF experiment shows that the $2^1A''$ surface does not substantially influence the $HONO_2$ photodissociation dynamics until the single-photon excitation energies approach 40000 cm^{-1} [14]. This is consistent with the above conjecture that the NO$_2$($\widetilde{X}^2$A$_1$) channel might be the major pathway at energy well below 40000 cm^{-1}. As photolysis energy increases, the excitation to the $2^1A''$ state becomes more important, therefore the electronically excited NO_2 channel should become a major pathway. This is supported by the previous photolysis experiment of HNO_3 at 248 nm, in which the dissociation on the $2^1A''$ surface was dominant [34]. Since two excited $1^1A''$ and $2^1A''$ surfaces couple with each other, excitation to the $2^1A''$ state will also lead to the ground state NO_2 product channel. This might be the reason that the two channels cannot be separated well in the photodissociation experiment.

D. Angular distributions

The angular distribution was derived from the images of OH from the photolysis of $HONO_2$. The anisotropy parameters β are obtained by fitting the angular distributions to Eq.(1). The polarization direction of the probe laser was changed to check the angular momentum polarization of the OH fragment. A negligible change in the OH angular distribution is observed, suggesting that there is little or no polarization effect on the dissociation process. Figure 5 shows the angular distributions of OH at different rotational states from the photodissociation of $HONO_2$ at 37023.3 cm^{-1} excitation energy. As seen from Fig.5, β equals 1.07±0.16 for the OH $R_1(6)$ detection and 0.47±0.02 for the OH $P_1(4)$ and $R_1(1)$ detection from the photolysis of $HONO_2$ at 37023.3 cm^{-1}. This is similar to the experimental results at the excitation energy of 35714.3 cm^{-1} (excita-

DOI:10.1088/1674-0068/22/02/191-196

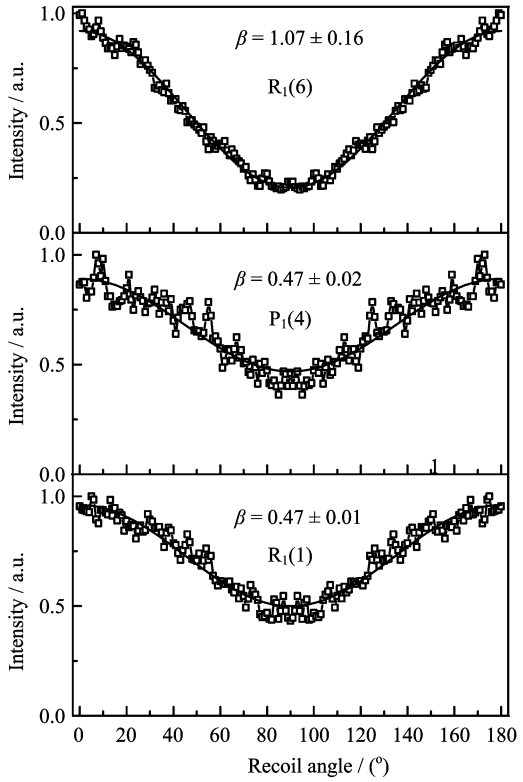

FIG. 5 Angular distributions of OH in the different rotational states from the photolysis of $HONO_2$ at 37023.3 cm^{-1}. The solid lines indicate the fit to the anisotropy parameter β according to Eq.(1).

tion to $1^1A''$ state) using the LIF technique [17].

The geometry change from the planar ground state to the pyramidal excited electronic state gives rise to the vibronic excitation in A″ symmetry. The vibrationally coupled A″←A′ perpendicular electronic transition leads to the parallel angular distribution of OH fragments [15,17]. The parallel distribution suggests that the dissociation process is faster than the rotational period of $HONO_2$ molecule. Anisotropy parameter β measured for the OH product via the $R_1(6)$ transition is 1.09±0.13 at 37023.3 cm^{-1} excitation and decreases to 0.71±0.10 and 0.47±0.02 at 40939.2 and 44924.8 cm^{-1} excitation, respectively. At the excitation energy of 44924.8 cm^{-1}, the fast kinetic $NO_2(\widetilde{X}^2A_1)$ channel has a β of 0.69 compared with the slow $NO_2(\widetilde{A}^2B_2)/NO_2(\widetilde{X}^2A_1)$ channel of 0.47 in the $R_1(6)$ transition of OH. For the $P_1(4)$ transition of OH at the same photolysis energy, the values of β are 0.24±0.01 for $NO_2(\widetilde{A}^2B_2)/NO_2(\widetilde{X}^2A_1)$ and 0.67±0.04 for $NO_2(\widetilde{X}^2A_1)$.

From the above discussion, there are two dissociation pathways in competition in the UV photodissociation of $HONO_2$. The avoided crossing between the $1^1A''$ and $2^1A''$ surfaces in the C_s symmetry of $HONO_2$ makes the two surfaces correlate with the $NO_2(\widetilde{X}^2A_1)$ and $NO_2(\widetilde{A}^2B_2)$ channel respectively.

IV. CONCLUSION

Photodissociation dynamics of $HONO_2$ was studied using time-sliced ion imaging of the OH product with REMPI state-selective detection. The total kinetic energy release (TKER) spectra of OH+NO_2 were determined from the slice images of the OH product. The peak position in the TKER spectra remains at almost the same position at different photoexcitation energies. Two dissociation channels of $NO_2(\widetilde{X}^2A_1)$ and $NO_2(\widetilde{A}^2B_2)$ are likely present, which suggests that both $1^1A''$ and $2^1A''$ electronic states are involved in the excitation. The parallel angular distribution, relative to the photolysis laser polarization, in the OH+NO_2 channel from dissociation of $HONO_2$ suggests that the dissociation process is rather direct and fast, in comparison with rotational period of the HNO_3 molecule. The anisotropy parameter β is found to be dependent on the angular momentum of the OH product, as well as the photolysis energy.

V. ACKNOWLEDGMENTS

This work was supported by the National Natural Science Foundation of China, the Ministry of Sciences and Technology, and the Chinese Academy of Sciences.

[1] J. Matthews, A. Sinha, and J. S. Francisco, Proc. Natl. Acad. Sci. USA. **12**, 7449 (2005).
[2] M. E. Greenslade, M. I. Lester, D. C. Radenovic, A. J. A. van Roij, and D. H. Parker, J. Chem. Phys. **123**, 074309 (2005).
[3] M. P. J. van der loo and G. C. Groenenboom, J. Chem. Phys. **123**, 074310 (2005).
[4] M. Collard, P. P. Kerwin, and A. Hodgson, Chem. Phys. Lett. **179**, 422 (1991).
[5] E. De Beer, M. Koopmans, C. d. de Lange, Y. Wang, and W. Chupka, J. Chem. Phys. **94**, 7634 (1991).
[6] R. Forster, H. Hippler, K. Hoyermann, G. Rohde, and L. B. Harding, Chem. Phys. Lett. **183**, 465 (1991).
[7] J. Cutler, Z. He, and J. Sampson, J. Phys. B **28**, 4577 (1995).
[8] R. Wiedmann, R. Tonkyn, M. White, K. Wang, and V. McKoy, J. Chem. Phys. **97**, 768 (1995).
[9] C. McRaven, J. Alnis, B. Furneaux, and N. Shafer-Ray, J. Phys. Chem. A **107**, 7138 (2003).
[10] A. Sinha, R. L. Vander Wal, and F. F. Crim, J. Chem. Phys. **91**, 2929 (1989).
[11] G. H. Leu, C. W. Hwang, and I. C. Chen, Chem. Phys. Lett. **257**, 481 (1996).
[12] J. R. Huber, Chem. Phys. Chem. **5**, 1663 (2004).
[13] M. J. Krisch, M. C. Reid, L. R. McCunn, L. J. Butler, and J. Shu, Chem. Phys. lett. **397**, 21 (2004).

DOI:10.1088/1674-0068/22/02/191-196

[14] C. E. Miller and H. S. Johnston, J. Phys. Chem. **97**, 9924 (1993).
[15] J. Schliitter and K. Kleinermanns, Chem. Phys. Lett. **192**, 94 (1992).
[16] S. J. Baek, C. R. Park, and H. L. Kim, J. Photochem. Photobio. A **104**, 13 (1997).
[17] J. August, M. Brouard, and J. P. Simons, J. Chem. Soc. Faraday Trans. **284**, 587 (1988).
[18] G. S. Jolly, D. L. Singleton, D. J. Mckenney, and G. Paraskevopoulos, J. Chem. Phys. **84**, 6662 (1986).
[19] A. Schiffman, D. D. Nelson Jr, and D. J. Nesbitt, J. Chem. Phys. **98**, 6935 (1993).
[20] A. Jacobs, K. Kleinermanns, H. Kuge, and J. Wolfrum, J. Chem. Phys. **79**, 3162 (1983).
[21] H. Johnston and R. Graham, J. Phys. Chem. **77**, 62 (1973).
[22] R. Graham and H. Johnston, J. Phys. Chem. **82**, 254 (1974).
[23] Y. Y. Bai and G. A. Segal, J. Chem. Phys. **92**, 7479 (1990).
[24] A. T. J. B Eppink and D. H. Parker, Rev. Sci. Instrum. **68**, 3477 (1997).
[25] C. R. Gebhardt, T. P. Rakitzis, P. C. Sarmartzis, V. Ladopoulos, and T. N. Kitsopoulos, Rev. Sci. Instrum. **72**, 3848 (2001).
[26] J. J. Lin, J. Zhou, W. Shiu, and K. Liu, Rev. Sci. Instrum. **74**, 2495 (2003).
[27] D. Townsend, M. P. Minitti, and A. G. Suits, Rev. Sci. Instrum. **74**, 2530 (2003).
[28] J. Liu, F. Y. Wang, H. Wang, B. Jiang, and X. M. Yang, J. Chem. Phys. **122**, 104309 (2005).
[29] J. Liu, F. Y. Wang, H. Wang, B. Jiang, and X. M. Yang, Chin. J. Chem. Phys. **19**, 1 (2006).
[30] H. Wang, S. L. Liu, J. Liu, F. Y. Wang, B. Jiang, and X. M. Yang, Chin. J. Chem. Phys. **20**, 388 (2007).
[31] D. Q. Li, R. T. Carter, and J. R. Huber, Chem. Phys. Lett. **334**, 39 (2001).
[32] H. Parker and A. T. J. B Eppink, J. Chem. Phys. **107**, 2357 (1997).
[33] T. L. Myers, N. R. Forde, B. Hu, D. C. Kitchen, and L. J. Butler, J. Chem. Phys. **107**, 5361 (1997).
[34] T. L. Mazely, R. R. Friedl, and S. P. Sander, J. Chem. Phys. **100**, 8040 (1994).

DOI:10.1088/1674-0068/22/02/191-196